

PACS numbers: 75.25.+z; 67.65.+z; 32.80.Bx
DOI: 10.1070/QE2003v033n01ABEH002359

An optically polarised dense ^{3}He target as a spin filter for slow-neutron beams

N.N. Kolachevsky, Yu.V. Prokof'ichev, V.R. Skoi, I.I. Sobelman, V.N. Sorokin

***Abstract*. The possibility of polarising ^{3}He and preserving the polarisation in an external magnetic field of 0.05 Oe is demonstrated experimentally. A neutron filter with an extremely weak guiding field is fabricated for obtaining polarised neutron beams. The degree of polarisation equal to 25 % was obtained for 0.025-eV neutrons. Some fields of application of other polarised noble gases are considered. The cross section for cross-relaxation of nuclear polarisation in the ^{129}Xe – ^{131}Xe mixture is estimated.**

Keywords: *laser spin polarisation, spin filter, neutron polarisation.*

1. Introduction

The preparation of polarised states of atoms and nuclei (polarisation of the valence-electron spin $\boldsymbol{s}$ and polarisation of the nuclear spin $\boldsymbol{I}$) opens up a wide range of possibilities for precision experiments in the field of basic research in physics (the search and investigation of parity nonconservation and nuclear anapole moment in experiments with polarised atomic beams and the search for T invariance violation effects). Targets with polarised nuclei are important elements in experiments that are also aimed at solving a number of problems in nuclear physics.

The possibility of polarising the nuclear spin in gaseous ^{3}He is especially interesting. Such a gas at high pressures can serve as a very efficient polariser of neutrons over a wide energy range [1, 2]. This is possible because polarised ^{3}He nuclei absorb resonantly the neutrons whose spins are antiparallel to the spins of the ^{3}He nuclei. For the neutron energy $E_T = 0.0253$ eV (thermal point), the cross section $\sigma_{\rm res}$ for such a resonance absorption in the reaction ^{3}He(n, p)^{3}H is $\sim 5370 \times 10^{-24}$ cm^2. As the neutron energy increases, the cross section $\sigma_{\rm res}$ decreases inversely proportional to the velocity, but its value for energies below 10 eV remains several thousand times higher than the absorption cross section for neutrons whose spins are parallel to the nuclear spins of ^{3}He.

N.N. Kolachevsky, I.I. Sobelman, V.N. Sorokin P.N. Lebedev Physics Institute, Russian Academy of Sciences, Leninskii prosp. 53, 119991 Moscow, Russia;
Yu.V. Prokof'ichev, V.R. Skoy Joint Institute for Nuclear Research, I.M. Frank Neutron Physics Laboratory, 141980 Dubna, Moscow region

Received 10 June 2002

Kvantovaya Elektronika **33** (1) 18 – 24 (2003)
Translated by Ram Wadhwa

When a target is large enough and the concentration of the polarised ^{3}He nuclei is high, the outcoming beam is enriched with neurons whose spins are parallel to nuclear spins.

In recent years, a new promising trend of using noble gases with polarised nuclei in medicine emerged suddenly. It was shown that the inhalation of a polarised noble gas makes it possible to carry out diagnostics of the lungs by NMR tomographic technique (see, for example, [3, 4]).

The development of techniques for obtaining spin-polarised nuclei has a long history (see, for example, review [5]). A very high polarisation of gases is obtained by cooling them to temperatures below 1 K in magnetic fields of strength $\sim 10^5$ Oe. However, this method cannot be used efficiently in all cases, since an extremely weak (and in some cases even zero) magnetic field is required in a whole range of precision experiments involving polarised nuclei. In addition, it is also desirable to ensure the possibility of rapid reversal of the spin orientation, which can be realised easily in gas targets polarised by optical methods that do not require the application of a strong magnetic field. In this case, the spin orientation can be reversed at a rather high frequency during adiabatic magnetisation reversal.

Optical methods of polarisation of nuclear spins (especially, the spin of the ^{3}He nucleus) were developed much later than cryogenic methods. Modern laser technology was required for these methods. The spin of the ^{3}He nucleus can be polarised in two ways. The first of these involves orientation of the metastable ^{3}He atoms in the $2\,^3S_1$ state in a high-frequency discharge during absorption of circularly polarised radiation at 1.083 μm (the $2\,^3S \rightarrow 2\,^3P$ transition),

$$^3\mathrm{He}(2\,^3S) + n\hbar\omega \rightarrow {}^3\mathrm{He}\uparrow(2\,^3S) \qquad (1)$$

followed by a transfer of polarisation in collisions with a resonance transfer of excitation,

$$^3\mathrm{He}\uparrow(2\,^3S) + {}^3\mathrm{He}(1\,^1S_0) \rightarrow {}^3\mathrm{He}\uparrow(1\,^1S_0) + {}^3\mathrm{He}(2\,^3S). \qquad (2)$$

In the second method, the optical polarisation of the electron spins of alkali metal atoms A is first realised at the resonance $^2S_{1/2} \rightarrow {}^2P_{1/2}$ transition (D_1-line),

$$\mathrm{A} + n\hbar\omega \rightarrow \mathrm{A}\uparrow. \qquad (3)$$

In subsequent collisions with noble gas atoms B whose nuclei have a nonzero spin, the electron spin polarisation is transferred to the nuclear spin of a B atom. This method

was tested long before the creation of lasers, but its application began only after the appearance of high-power lasers. A considerable role in the development of this method was played by the research carried out by Happer and his co-workers [1, 2]. Both these methods have their own advantages and drawbacks as far as the polarisation of ^{3}He is concerned.

For example, the concentration of ^{3}He is limited when the first method is applied because nuclear spin polarisation begins upon optical pumping of a ^{3}He atom in the metastable $2\,^3S$ state. A high density of the metastable state cannot be created at a high pressure of the order of 1 atm or more. However, the efficiency of transfer of polarisation of pumping photons to nuclear spins is very high.

While using the second method, it is preferable to work at ^{3}He concentrations corresponding to pressures 1 – 10 atm. The efficiency of photon polarisation transfer to nuclear spins is low in this case. This is due to a relatively high probability of collisional relaxation of the polarisation of alkali metal atoms in the ground $^1S_{1/2}$ state. The mechanisms of such relaxation were discussed in detail in a number of papers, including [6]. The main results for the Rb – ^{3}He mixture can be summarised as follows. Since the rate constant of the process of polarisation transfer from the electron spin to ^{3}He atomic nuclei is very low ($\langle v\sigma\rangle \sim 10^{-19}$ cm^3 s^{-1}), the electron spin relaxation during collision of two polarised Rb atoms plays the decisive role:

$$\mathrm{Rb}\uparrow + \mathrm{Rb}\uparrow \rightarrow \mathrm{Rb}\uparrow + \mathrm{Rb}\downarrow. \tag{4}$$

Under the conditions of the experiment [1], the electron spin relaxation rate for a rubidium concentration $n_{\mathrm{Rb}} = 10^{15}$ cm^{-3} was $\Gamma \simeq 10^3$ s^{-1}. The specific pump power required for polarisation of Rb vapour in a cell of volume V is $W/V \simeq 0.2$ W cm^{-3}, where W is absorbed laser-beam power. Note that only a very small part ($\sim 1\%$) of the pump power W is spent on polarising ^{3}He, the rest of the energy being dissipated due to spin relaxation.

Let us present the main experimental data [1, 2] on the polarisation of ^{3}He in the Rb – ^{3}He mixture. A ring dye laser pumped by a krypton ion laser produced an output power of 1 W at a wavelength of 795 nm of the resonance D_1 line in a Rb atom. In a cell of volume $V \sim 6$ cm^3 with a cross-sectional area of 0.65 cm^2, the polarisation of the ^{3}He nuclear spin was about 70 % for $n_{\mathrm{He}}L \approx 3 \times 10^{20}$ cm^{-2} (where L is the length of the cell and n_{He} is the helium concentration). The results [1, 2] played an exceptionally important role in demonstrating the efficiency of using the optical method. However, it turned out that the pump power must be increased considerably in a large number of experiments involving polarised nuclei.

Note that ring dye lasers pumped by ion lasers (Ar^+ and Kr^+ lasers) produce an output power ~ 1 W, while Ti : sapphire lasers can emit up to 3 – 4 W within the shape of the D_1 line of Rb and K atoms. A further increase in the output power was achieved using pumping by semiconductor lasers. Linear diode arrays tuned to the D_1 line of Rb, which ensure the required pumping without a Ti : sapphire laser at all, seem to offer considerable promise. The pump power can be increased up to 10 – 50 W by using such a direct method of pumping.

A characteristic feature of the method is that the spectral linewidth of the radiation from a linear diode array is considerably larger (by approximately an order of magnitude) than the width of the D_1 absorption line of Rb. This necessitated certain variations in the experimental technique (see, for example, Refs [7, 8]). First, the maximum possible pressure of ^{3}He (more than 3 atm) was employed to ensure a considerable collision broadening of the D_1 line. (For a pressure of ^{3}He equal to 4 atm, the collision linewidth at a temperature of 190 °C was ~ 2.5 cm^{-1}.) In addition, as the pressure of ^{3}He increases, the efficiency of the polarisation transfer from rubidium to helium also increases. Second, pumping was performed at a considerable optical depth of rubidium vapour in the region of the D_1 line. This made it possible to use a considerable part of the absorption profile wings for pumping and, consequently, about 80 % of the diode array power emitted in the linewidth of 2.4 nm.

We present below the results of the experiments on the polarisation of a beam of thermal neutrons by a helium target, which was polarised by pumping Rb by 15 W of 795-nm radiation from a diode array.

A constant magnetic field $B_\parallel$ whose direction coincides with the laser beam is required for optical pumping of rubidium. This is caused by the requirement to split the magnetic sublevels of the ground state of the atom. Estimates show that even the weakest magnetic field is sufficient for complete splitting of the sublevels and, hence, for optical pumping. Consequently, the external magnetic field can be strongly decreased compared to the conventionally used fields. For example, in experiments with a neutron beam when a polariser and a target are oriented mutually orthogonally, the precession of neutron polarisation appears in crossed fields in the region between the polariser and the target, which gives rise to a number of spurious systematic effects. The precession frequency is low in weak fields, and hence the systematic effects associated with it are also insignificant.

On the other hand, a homogeneous external magnetic field is necessary for preventing the depolarisation of ^{3}He nuclei due to the inhomogeneity of the laboratory field. The characteristic nuclear relaxation time τ_{m} related to the magnetic inhomogeneities is described by the expression [9]

$$\frac{1}{\tau_{\mathrm{m}}} \approx D_{\mathrm{He}} \left(\frac{\nabla B_\perp}{B_\parallel} \right)^2, \tag{5}$$

where D_{He} is the diffusion coefficient of helium, and $B_\perp$ and $B_\parallel$ are the components of the field perpendicular and parallel to the direction of nuclear polarisation, respectively.

Both the problems (decreasing the guiding field strength and the influence of the external fields) can be solved simultaneously by placing the cell in a cylindrical magnetic shield. Since the screening factor $S_\perp$ of the field component perpendicular to the shield axis is usually much larger than the longitudinal screening factor $S_\parallel$, the shield 'lines up' the field along its axis. Therefore, by making the shield axis coincide with the direction of the laser beam, we can create a very small residual homogeneous field at the position of the cell.

Because the gradients of the external fields are usually small, we can assum that

$$B_\parallel^{\mathrm{int}} = \frac{B_\parallel^{\mathrm{ext}}}{S_\parallel}, \quad \nabla B_\perp^{\mathrm{int}} \approx \frac{\nabla B_\perp^{\mathrm{ext}}}{S_\perp}, \tag{6}$$

where the superscripts 'int' and 'ext' correspond to the field components inside and outside the shield, respectively. In this case, expression (6) for the cell inside the shield takes the form

$$\frac{1}{\tau_{\mathrm{m}}^{\mathrm{int}}} = \frac{1}{\tau_{\mathrm{m}}^{\mathrm{ext}}}\left(\frac{S_{\parallel}}{S_{\perp}}\right)^2 \ll \frac{1}{\tau_{\mathrm{m}}^{\mathrm{ext}}}. \quad (7)$$

Thus, a magnetic shield makes it possible to obtain a weak and rather homogeneous field and to considerably decrease the effect of the inhomogeneous surrounding fields. In addition, when a shield is used, no external sources of fields in the form of rings or solenoids are required, and the Earth's magnetic field is quite sufficient for the experiments.

In a number of practical applications, cross polarisation is also important along with the transfer of the atomic polarisation of alkali metals to the nuclei of noble metals. This effect can take place, for example, in binary mixtures of different inert gases or in different isotopes of the same gas. It is actually the mutual exchange (transfer) of nuclear polarisation between the components of the mixture. If the rate constant corresponding to the transfer is small, the components virtually do not interact, and the mixture consists of two separate spin subsystems. Otherwise, a complex dynamic system is formed, in which one of the components may play the role of a 'spin reservoir' for the other. For example, in the experiment KaTRIn [10] on verification of time invariance in the interaction of polarised neutrons with polarised nuclei, it is interesting to study the spin exchange processes in the $^{129}Xe - ^{131}Xe$ mixture intended for use as a polarised target. This question is studied in detail in Appendix.

2. Experimental setup

To verify the above conclusions, we performed experiments with a slow neutron beam from the IBR-30 reactor at the I.M. Frank Neutron Physics Laboratory at the Joint Institute for Nuclear Research. A schematic of the neutron polariser is shown in Fig. 1. The neutron polariser, which served as the target, was a spherical cell of diameter 3 cm made of Corning 1720 aluminium silicate glass. This glass is chemically inert with respect to hot rubidium vapour and contains small amounts of ferromagnetic and paramagnetic impurities, which are usually responsible for a rapid relaxation of the nuclear polarisation in collisions of polarised atoms with the cell walls. The cell was filled at the stand and sealed off. It contained a small amount of metallic rubidium, nitrogen at a pressure of 70 Torr, and ^{3}He whose concentration corresponded to the gas density at a pressure slightly lower than atmospheric and at the liquid nitrogen temperature. The nuclear polarisation lifetime for this target was first measured [8] at the Lebedev Physics Institute, and was found to be 36 ± 2 min. Such a rather short lifetime is explained by the fact that no fine filters were used for ^{3}He purification while filling the cell.

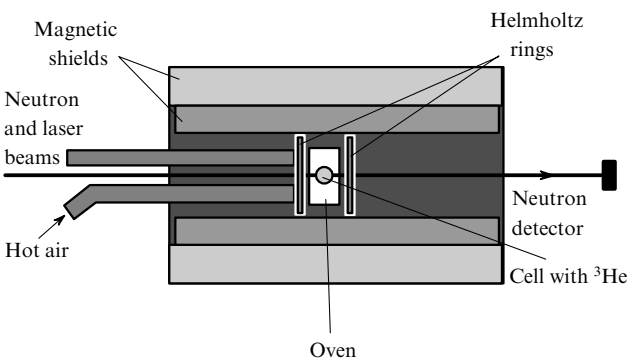

Figure 1. Schematic of the neutron beam experiment.

In the neutron beam experiment, the target was placed inside an aluminium box oven and was heated to a temperature of about 190 °C by blowing hot air from a blower. This temperature corresponds to the optimal concentration $(4-8)\times 10^{14}$ cm^{-3} of rubidium vapour. The oven walls also shielded the target from external alternating fields. Two cylindrical magnetic shields were mounted outside coaxially with the laser and neutron beams. Both shields were made of permalloy of thickness 0.5 mm, were 67 cm in length, and had diameters of 38 and 44 cm. Coils for demagnetisation were wound on the shields. Demagnetisation was carried out one day before the experiment to ensure the damping of relaxation processes in the shield material. The residual magnetic field at the centre (i.e., at the site of the target) was found to be longitudinal and equal to 0.05 Oe. A pair of small Helmholtz coils, capable of producing a magnetic field up to 7 Oe, were installed symmetrically outside the oven.

Fig. 2 shows the optical scheme for irradiating the target by a circularly polarised laser beam for pumping rubidium vapour and for controlling the spectrum of radiation passing through the target. We used an A015-795-FCPS diode laser (OptoPower Co.), whose radiation was outcoupled through a 23-fibre bundle of diameter 1.5 mm. The output radiation was not polarised, and its power was 15 W within a solid angle with a cone opening of 12° at the $1/e^2$ level. The emission spectrum had a complex shape and a total width of about 2.4 nm. The optimal tuning to the absorption line of rubidium was provided by adjusting the temperature of the diode laser.

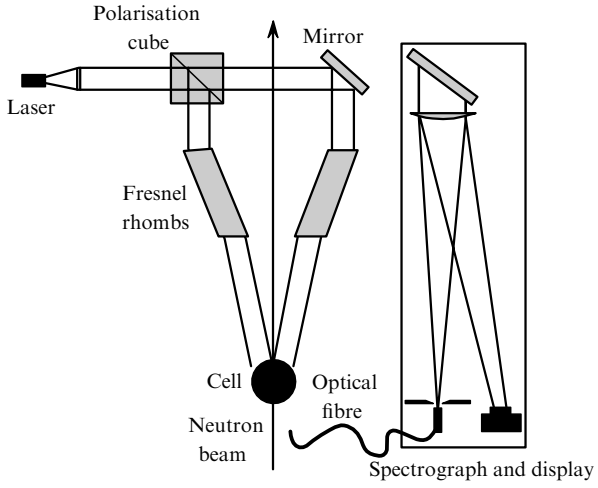

Figure 2. Optical pumping diagram.

The laser beam was collimated by a lens and split by a polarisation cube into two linearly polarised beams with mutually orthogonal polarisation planes. Linear polarisation was transformed into circular polarisation with the help of Fresnel rhombs. Both beams crossed in the cell volume at

an angle not exceeding 4°. The diameter of the beams at the target could be varied from 2 to 4 cm by moving the lens. In the beam transmitted through the target, the end of an optical fibre was placed through which the radiation entered a 30-cm spectrometer with a CCD array mounted instead of the exit slit. The spectrometer showed the radiation in the range from 792.7 to 797.3 nm with a resolution of 0.05 nm.

The number of neutrons passing through the target with polarisation p_{He} is

$$N = N_0 \exp[-\sigma_{\mathrm{res}}(E) n_{\mathrm{He}} L] \cosh[p_{\mathrm{He}} \sigma_{\mathrm{res}}(E) n_{\mathrm{He}} L]$$

$$= N_1 \cosh[p_{\mathrm{He}} \sigma_{\mathrm{res}}(E) n_{\mathrm{He}} L], \quad (8)$$

where E is the kinetic energy of neutrons; N_0 is the number of neutrons incident on the target; and N_1 is the number of neutrons passing through a target with unpolarised ^{3}He. The polarisation of the neutron beam coming from the target is described by the expression

$$p_{\mathrm{n}} = \tanh[p_{\mathrm{He}} \sigma_{\mathrm{res}}(E) n_{\mathrm{He}} L]. \quad (9)$$

The neutron polarisation was measured in the experiment using the standard time-of-flight technique. The polarisation was estimated from the expression [see Eqn (8)]

$$p_{\mathrm{n}} = \left[1 - \left(\frac{N_0}{N}\right)\right]^{1/2}. \quad (10)$$

The neutron beam was collimated in such a way that it passed between the optical elements shown in Fig. 2 without touching them.

A fission chamber with the ^{235}U isotope was used as the neutron detector. Resonances in the cross section for neutron absorption in ^{235}U played the role of 'natural' energy points while determining the neutron polarisation. For statistical normalisation of the data measured at different instants of time, we used the high-energy part of the neutron spectrum in the range from 7.89 to 93.46 eV. The cell used in the experiment polarises the beam very weakly ($p_{\mathrm{n}} \ll 1\%$) in this energy range.

Measurements were made in two stages, with and without the Helmholtz coils. The guiding field was 3 Oe in the former case and 0.05 Oe (residual field in the shield) in the latter case. Before starting the second stage of measurements (in zero field), the ^{3}He polarisation was destroyed by a small permanent magnet to restore the initial state. In each case, the measurement of the neutron spectra began 1.5 hours after the beginning of pump, when the polarisation of ^{3}He was saturated.

In addition to the main measurements, we also measured the spectra of neutrons passing through the cell with nonpolarised helium and of an open neutron beam (without the cell), as well as the background spectrum. The latter was recorded by inserting 0.5 mm-thick cadmium plate in the beam to absorb thermal neutrons.

3. Experimental results

Fig. 3 shows the results of measurement of neutron polarisation as a function of the neutron energy with and without the field. One can see that both polarisations are in good mutual agreement within the statistical error. Thus, the practical possibility of optical pumping of Rb vapour, polarisation, and storage of polarised ^{3}He in a weak magnetic field was established.

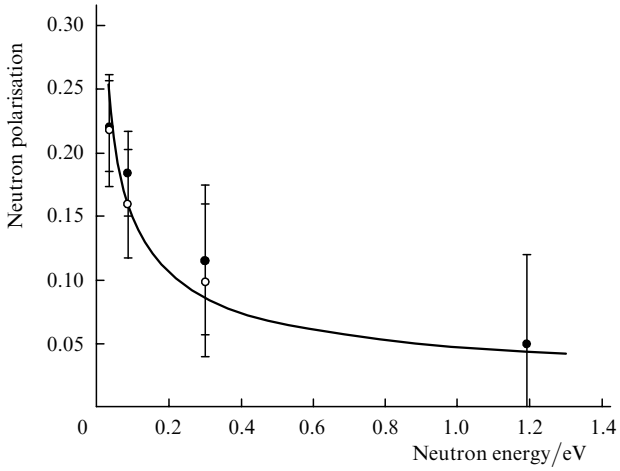

Figure 3. Dependences of the polarisation of neutrons on their energy with (dark circles) and without (open circles) Helmholtz coils. The solid curve is fitting for $p_{\mathrm{He}} = 0.30 \pm 0.03$.

The pressure P of ^{3}He in the cell was determined by fitting the quantity $\exp[-P n_{\mathrm{L}} (E_T/E)^{1/2} \sigma_{\mathrm{res}}(E_T) x]$ (where n_{L} is the Loschmidt number and x is the effective thickness of the cell) to the transmission (the ratio of the spectrum of neutrons passing through the cell with nonpolarised helium to the open beam spectrum). The role played by the absorption of neutrons by the cell walls themselves was also taken into account during fitting because aluminium silicate glass contains about 5 % B_2O_3. The natural mixture of boron isotopes contains 19.8 % ^{10}B which is a very strong absorber of thermal neutrons. This contribution was taken into account from the results of simulation using standard computer programs.

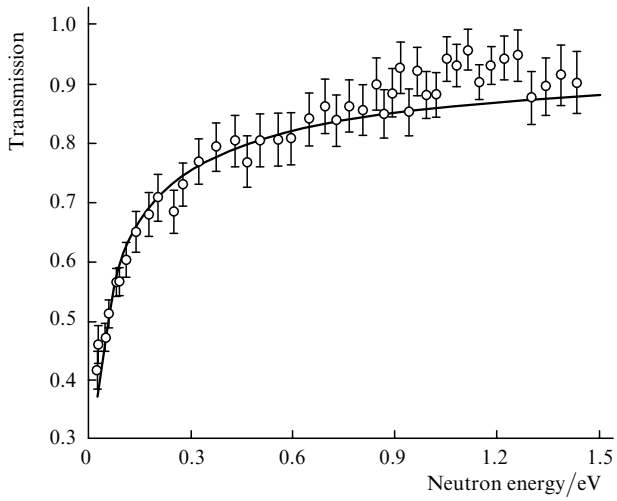

Figure 4. Transmission of neutrons for a cell with nonpolarised ^{3}He taking into account the correction due to absorption in the walls (circles). The solid curve is fitting for $P = 3.40 \pm 0.02$ atm.

Fig. 4 shows the transmission of neutrons through a cell with nonpolarised helium after taking into account the absorption in the cell walls. The figure also shows the curve obtained by fitting and corresponding to a ^{3}He pressure equal to 3.40 ± 0.02 atm. This value corresponds to the filling of the cell at liquid nitrogen temperature.

4. Conclusions

Thus, we have demonstrated the possibility of optical pumping of Rb vapour, polarisation of ^{3}He, and conservation of the polarisation in a weak (0.05 Oe) guiding magnetic field. The prototype of a new modification of the neutron filter for obtaining polarised neutron beams was created. It is supposed to use the measurements of the degree of polarisation of ^{3}He in this cell as a standard for making new cells and for determining their parameters by the NMR technique. The latter circumstance allows one to avoid the calibration of ^{3}He polarisation with respect to the NMR signal from water protons, which is quite complicated due to a weak signal.

We intend to use the experience gained by us in the course of our investigations as well as the techniques adopted by us to produce in future a full-scale KaTRIn setup and to carry out experiments aimed at detecting the violation of time invariance in the interactions between polarised neutrons and polarised nuclei.

Acknowledgements. The authors thank Sh. Zeinalov and A.V. Sermyagin for their help in neutron beam measurements and I.Yu. Tolstikhina for carrying out numerical calculations. This work was partially supported by the Russian Foundation for Basic Research (Grant Nos 00-15-96586 and 02-02-16980), the Federal programme 'Integratsiya' (Grant No. B-0049), and the Alexander Humboldt Foundation.

Appendix

Interaction of nuclear magnetic dipoles

The Hamiltonian of the dipole–dipole interaction between nuclear spins $\boldsymbol{I}_1$ and $\boldsymbol{I}_2$ has the form [11]

$$H' = Ag_1g_2[3(\boldsymbol{I}_1\boldsymbol{n})\boldsymbol{n} - \boldsymbol{I}_1]\boldsymbol{I}_2, \tag{A1}$$

where

$$A = -\frac{1}{2}\alpha^2\left(\frac{m_e}{m_p}\right)^2\left(\frac{a_0}{R}\right)^3\frac{e^2}{2a_0}; \tag{A2}$$

$\alpha = e^2/\hbar c \simeq 1/137$; a_0 is the atomic unit of length; e^2/a_0 is the atomic unit of energy; m_e and m_p are the electron mass and the proton mass, respectively; g_1 and g_2 are the gyromagnetic ratios (g-factors) for nuclei 1 and 2, respectively; R is the spacing between nuclei 1 and 2; and $\boldsymbol{n}$ is the unit vector directed along the vector $\boldsymbol{R}$.

A rigorous calculation of the effective cross section for the polarisation transfer between nuclei 1 and 2,

$$\sigma(m_1, m_2 \to m_1 - 1, m_2 + 1), \tag{A3}$$

where m_1 and m_2 are the magnetic quantum numbers, requires the solution of the problem on the elastic scattering of nuclei 1 and 2 taking into account the weak spin-spin interaction potential (A1) within the framework of the perturbation theory. Rough estimates of the cross section (A3) can be obtained by using a simpler (semiclassical) procedure assuming that

$$\sigma(m_1, m_2 \to m_1 - 1, m_2 + 1) = 2\pi\int_0^{\rho_0} W(\rho)\rho\mathrm{d}\rho, \tag{A4}$$

where

$$W(\rho) = \frac{1}{\hbar^2}|\langle m_1, m_2|H'|m_1 - 1, m_1 + 1\rangle|^2\left(\frac{\rho}{v}\right)^2 \tag{A5}$$

is the dimensionless probability of the polarisation exchange ($m_1,\ m_2 \to m_1 - 1,\ m_2 + 1$) during collisions of atoms 1 and 2 with an impact parameter ρ and a velocity v over a time $\tau = \rho/v$. The impact parameter ρ_0 is expressed in terms of the elastic scattering cross section σ_{el} as:

$$\rho_0 \simeq \left(\frac{\sigma_{el}}{\pi}\right)^{1/2}. \tag{A6}$$

Let us test this method of estimating the cross section (A4) and probability (A5) by the example of the processes of polarisation transfer from the electron spin $\boldsymbol{s}$ of the Rb atom to the nuclear spin $\boldsymbol{I}$ during collisions of Rb with ^{3}He and Rb with ^{129}Xe. Reliable experimental data are available for these processes.

In the above-mentioned collisions, the nuclear spin $I = 1/2$, and the main role in the polarisation transfer is played by the contact interaction whose potential is proportional to $\boldsymbol{sI}$. According to [11], we have

$$H' = \frac{8\pi}{3}\alpha^2 g_1\left(\frac{m_e}{m_p}\right)\frac{e^2}{2a_0}a_0^3|\psi(0)|^2\boldsymbol{sI}, \tag{A7}$$

$$\langle m_s, m_I|\boldsymbol{sI}|m_s - 1, m_i + 1\rangle$$

$$= 3/2\left|\begin{pmatrix} 1/2 & 1 & 1/2 \\ -1/2 & 1 & -1/2 \end{pmatrix}\right|^2 = \frac{1}{2}, \tag{A8}$$

$$\langle m_s, m_I|H'|m_s - 1, m_I + 1\rangle = \frac{2\pi}{3}\alpha^2 g_I\left(\frac{m_e}{m_p}\right)\frac{e^2}{a_0}a_0^3|\psi(0)|^2,$$

where $\psi(0) = \psi(R = 0)$ is the electron wave function of the Rb atom, describing its motion in the field of the nucleus of a noble gas atom, taken for $R = 0$.

For collisions of Rb with ^{3}He, we have $g_I = 4.26$ [12]. Hence, we obtain from (A5)

$$W(\rho) = 6.5 \times 10^{-14}\left(\frac{v_0}{v}\right)^2\left(\frac{\rho}{a_0}\right)^2\left[a_0^3|\psi(0)|^2\right]^2$$

$$= 7.8 \times 10^{-8}\left(\frac{\rho}{a_0}\right)^2\left[a_0^3|\psi(0)|^2\right]^2, \tag{A9}$$

where $v_0 = e^2/\hbar = 2.19 \times 10^8$ cm s^{-1} is the atomic unit of velocity and $v = 2 \times 10^5$ cm s^{-1} corresponds to the temperature $T \simeq 500$ K.

The integral with respect to ρ in (A4) can be evaluated by taking into account that ρ_0 (A6) approximately corresponds to the closest approach of an electron of a Rb atom

to the nucleus of a ^{3}He atom. Assuming that $\sigma_{el} \sim 10^{-15}$ cm^2, we obtain $\rho_0 = 1.8 \times 10^{-8}$ cm $\simeq 3.4a_0$.

In order to evaluate the factor $a_0^3|\psi(0)|^2$, we calculated $|\psi(0)|^2$ for a $2s$ electron in the excited $1s2s$ state of a He atom, a $1s$ electron in the ground $1s^2$ state of a He atom, and a $2s$ electron in the ground $1s^2\,2s$ state of a Li atom. The latter two cases are test cases, since they provide a reliable upper estimate of the factor $a_0^3|\psi(0)|^2$. For a $1s$ electron in the He atom, the mean square radius of the electron orbit $r \simeq a_0 = 0.53 \times 10^{-8}$ cm, which is much smaller than the value of ρ_0; for a Li atom, charge $Z = 3$ must be taken instead of $Z = 2$ for a He atom. Recall that $|\psi_{ns}(0)|^2 = Z^3/(\pi a_0^3 n^3)$ for a hydrogen atom, where n is the principal quantum number.

Calculations were performed by using the RCN program from the COWAN software package [13], one of the best programs in the multiconfigurational Hartree–Fock method. As a result, we obtain:

$$r = 4.8a_0,\ \ a_0^3|\psi_{2s}(0)|^2 = 0.103 \ \ \text{for} \ \ \text{He}(1s2s),$$

$$r = 1.08a_0,\ a_0^3|\psi_{1s}(0)|^2 = 1.75 \ \text{for} \ \text{He}(1s^2), \tag{A10}$$

$$r = 4a_0,\ \ a_0^3|\psi_{2s}(0)|^2 = 0.18 \ \ \text{for} \ \ \text{Li}(2s^2\,2s).$$

The radius $r = 4.8a_0$ is close to $\rho_0 = 3.4a_0$. Hence, we substitute into (A9) the most probable value $[a_0^3|\psi(0)|^2]^2 = 0.01$ to obtain

$$W(\rho) = 7.8 \times 10^{-10}\left(\frac{\rho}{a_0}\right)^2. \tag{A11}$$

It follows from (A4) that

$$\sigma(m_s, m_I \to m_s - 1, m_I + 1) = 3.8 \times 10^{-10}\pi\rho_0^2\left(\frac{\rho_0}{a_0}\right)^2$$

$$\simeq 4.3 \times 10^{-24}\ \text{cm}^2. \tag{A12}$$

The cross section (A12) corresponds to the spin polarisation exchange process $\text{Rb}\uparrow + {}^3\text{He}\downarrow \to \text{Rb}\downarrow + {}^3\text{He}\uparrow$. The experimental data refer to the process $\text{Rb}\uparrow + {}^3\text{He} \to \text{Rb} + {}^3\text{He}\uparrow$ whose cross section is half the cross section (A12). Taking this into account, we find that the polarisation cross section of ^{3}He in a mixture with totally polarised Rb is

$$\sigma \simeq 2.15 \times 10^{-24}\ \text{cm}^2. \tag{A13}$$

For $v = 2 \times 10^5$ cm s^{-1}, the rate constant of such a polarisation process is

$$\langle v\sigma\rangle = 4.3 \times 10^{-19}\ \text{cm}^3\ \text{s}^{-1}. \tag{A14}$$

According to Ref. [2], we have

$$\langle v\sigma\rangle_{\text{exp}} = 1.2 \times 10^{-19}\ \text{cm}^3\ \text{s}^{-1}. \tag{A15}$$

One can see that the theoretical estimate (A4) is in satisfactory agreement with the experiment. Recall that in the method used for estimation, the cross section σ depends in fact on the elastic scattering cross section: $\sigma \propto \sigma_{el}^2$ (A12). All that is required for the coincidence of the estimates (A14) and (A15) is to halve the quantity σ_{el} and equate it to 0.53×10^{-15} cm^2 instead of 10^{-15} cm^2, as was done above.

For collisions of Rb and ^{129}Xe atoms ($I = 1/2$), the substitution:

$$g_I({}^3\text{He}) = 4.26 \to g_I({}^{129}\text{Xe}) = -1.554,$$

$$v^2(\text{Rb} - {}^3\text{He}) = 4 \times 10^{10}\ (\text{cm s}^{-1})^2 \to v^2(\text{Rb} - {}^{129}\text{Xe})$$

$$= 0.43 \times 10^{10}\ (\text{cm s}^{-1})^2$$

should be made in (A9).

As a result, we obtain

$$W(\rho) = 9 \times 10^{-8}\left(\frac{\rho}{a_0}\right)^2\left[a_0^3|\psi(0)|^2\right]^2. \tag{A16}$$

The factor $a_0^3|\psi(0)|^2$ in (A16) can be estimated by calculating $W(\rho)$ for the $5s$ and $6s$ electrons in the ground state of the Cs atom. The nuclear charges in Xe and Cs atoms are almost identical (54 and 55). The screening of the nuclear charge by filled electron shells is also identical, and hence we have

$$r = 6.3a_0,\ \ a_0^3|\psi_{6s}(0)|^2 = 2 \ \ \text{for} \ \ \text{Cs}(6s),$$

$$r = 1.94a_0,\ \ a_0^3|\psi_{5s}(0)|^2 = 33 \ \ \text{for} \ \ \text{Cs}(5s). \tag{A17}$$

Using the same values of $\sigma_{el} = 10^{-15}$ cm^2, $\rho_0 = 3.4a_0$ as for the collisions of Rb with ^{3}He and comparing the mean square radii $r = 6.32a_0$ and $1.94a_0$ with ρ_0, we find that $a_0^3|\psi(0)|^2 \simeq 5 - 7$. Hence, for the process

$$\text{Rb}\uparrow + {}^{129}\text{Xe} \to \text{Rb} + {}^{129}\text{Xe}\uparrow,$$

the rate constant of the reaction is

$$\langle v\sigma\rangle = (1 - 2) \times 10^{-16}\ \text{cm}^3\ \text{s}^{-1}, \tag{A18}$$

which is also in satisfactory agreement with the experimental results (see, for example, Ref. [14]).

Let us now estimate the cross section for polarisation transfer between two nuclear spins, for example, during the collision of two isotopes ^{129}Xe and ^{131}Xe. In this case, a contact interaction of type (A7) is impossible due to the electrostatic repulsion between the nuclei, and we must proceed from relations (A1) and (A2). We consider only the case when one of the nuclear spins is $I1 = 1/2$. Let us introduce the notation $\boldsymbol{I}_1 = \boldsymbol{i}$, $\boldsymbol{I}_2 = \boldsymbol{I}$ ($i = 1/2$). In this case, expression (A1) can be rewritten as a tensor product of irreducible tensor operators [11]:

$$H' = -Ag_i g_I\sqrt{10}\sum_{\lambda}(-1)^{\lambda}\left[C^2 \times i^1\right]^1_{\lambda} I_{-\lambda}, \tag{A19}$$

where

$$\left[C^2 \times i^1\right]^1_{\lambda} = \sum_{\lambda,\sigma,\sigma'}(-1)^{-1-\lambda}\sqrt{3}\begin{pmatrix} 2 & 1 & 1 \\ \sigma & \sigma' & -\lambda \end{pmatrix} C^2_{\sigma} i^1_{\sigma'};$$

$$C_\sigma^2 = \left(\frac{4\pi}{3}\right)^{1/2} Y_{2\sigma}(\theta_{\boldsymbol{R}}\varphi_{\boldsymbol{R}}). \quad \text{(A20)}$$

The general expressions determining the irreducible tensor operators U_q^k, T_λ^r, their scalar products $U^k T^k = \sum_q (-1)^q U_{-q}^k T_q^k$, and tensor products $[U^k \times T^k]_\sigma^r$ can be found, for example, in Ref. [11]. By substituting (A20) into (A19), we obtain

$$H' = A g_i g_I \sqrt{30} \sum_{\lambda,\sigma,\sigma'} \begin{pmatrix} 2 & 1 & 1 \\ \sigma & \sigma' & -\lambda \end{pmatrix} C_\sigma^2 i_{\sigma'}^1 I_{-\lambda}. \quad \text{(A21)}$$

Consider the matrix element of the Hamiltonian H' for the process of transfer of polarisation exchange for spins $\boldsymbol{i}$ and $\boldsymbol{I}$, i.e., for the $m_i, m_I \to m_i - 1, m_I + 1$ transition, where m_i and m_I are the magnetic quantum numbers of the nuclear spins. Standard calculations of the sums containing 3j-symbols lead to the following result [11]:

$$\langle m_i, m_I | H' | m_i - 1, m_I + 1 \rangle$$

$$= A g_i g_I \sqrt{45} \left[I(I+1)(2I+1)\right]^{1/2} (-1)^{I-m_I} \left(\frac{4\pi}{3}\right)^{1/2} Y_{20} \quad \text{(A22)}$$

$$\times \begin{pmatrix} 2 & 1 & 1 \\ 0 & 1 & -1 \end{pmatrix} \begin{pmatrix} 1/2 & 1 & 1/2 \\ -1/2 & 1 & -1/2 \end{pmatrix} \begin{pmatrix} I & 1 & I \\ -m_I & -1 & m_i + 1 \end{pmatrix}.$$

By substituting the numerical values of the first two 3j-symbols into (A22), we obtain

$$\langle m_i, m_I | H' | m_i - 1, m_I + 1 \rangle$$

$$= -\left(\frac{1}{2}\right)^{1/2} A g_i g_I \left[I(I+1)(2I+1)\right]^{1/2} (-1)^{I-m_I}$$

$$\times \begin{pmatrix} I & 1 & I \\ -m_I & -1 & m_{I+1} \end{pmatrix} \left(\frac{4\pi}{3}\right)^{1/2} Y_{20}. \quad \text{(A23)}$$

In expression (A2) for the constant A, we can replace R by ρ because R is the spacing between the nuclei of colliding atoms. The dependence of A on ρ can be written approximately in the form $A(\rho) \simeq A(\rho_0) \simeq (a_0/\rho_0)^3$ for $\rho \leqslant \rho_0$ and $A(\rho) = (a_0/\rho)^3$ for $\rho \geqslant \rho_0$. Hence, expression (A5) can be written in the form

$$W(\rho) = 0.63 \times 10^{-24} \left(\frac{v_0}{v}\right)^2 g_i^2 g_I^2$$

$$\times \left[I(I+1)(2I+1) \left| \begin{pmatrix} I & 1 & I \\ -m_I & -1 & m_I + 1 \end{pmatrix} \right|^2 \right]$$

$$\times \left\langle \frac{4\pi}{3} Y_{20}^2 \right\rangle \left(\frac{a_0}{\rho_0}\right)^6 \frac{\rho^2}{a_0^2}, \quad \rho \leqslant \rho_0. \quad \text{(A24)}$$

While evaluating the angular factor $\langle (4\pi/3) Y_{20}^2(\theta_{\boldsymbol{R}}\varphi_{\boldsymbol{R}}) \rangle$, recall that the vector $\boldsymbol{R}$ is directed from the nucleus with spin $\boldsymbol{i}$ to the nucleus with spin $\boldsymbol{I}$. It can be concluded from the graphic view of the solid angle making the main contribution to the interaction that $\langle (4\pi/3) Y_{20}^2 \rangle \simeq 1$.

Let us estimate the cross-polarisation cross section σ in the mixture of isotopes ^{129}Xe–^{131}Xe at room temperature for $(v_0/v)^2 = 2 \times 10^8$. The spins and the g-factors of the isotopes are

$$i = 1/2, \quad g_i = -1.56 \quad \text{for} \quad {}^{129}\text{Xe},$$

$$I = 3/2, \quad g_I = +0.47 \quad \text{for} \quad {}^{131}\text{Xe}.$$

Calculation of the sum over $m = -3/2, -1/2, +1/2$ gives

$$I(I+1)(2I+1) \frac{1}{2I+1} \sum_m \left| \begin{pmatrix} I & 1 & I \\ -m & -1 & m+1 \end{pmatrix} \right|^2 = \frac{5}{4}.$$

Using expression (A4), we obtain the estimate (for $\pi\rho_0^2 = \sigma_{\text{el}} = 10^{-15}$ cm^2, $\rho_0 = 3.4 a_0$):

$$\sigma \simeq 0.5 \times 10^{-16} \pi a_0^2 \left(\frac{\pi a_0^2}{\sigma_{\text{el}}}\right) \simeq 0.5 \times 10^{-32} \left(\frac{\pi a_0^2}{\sigma_{\text{el}}}\right), \quad \text{(A25)}$$

which, as expected, is about $(m_e/m_p)^2$ times smaller than σ (A13).

References

1. Chupp T.E., Wagshul M.E., Coulter K.P., McDonald A.B., Happer W. *Phys. Rev. C*, **36**, 2244 (1987).
2. Coulter K.P., McDonald A.B., Happer W., Chupp T.E., Wagshul M.E. *Nucl. Instr. Meth. Phys. Research A*, **270**, 90 (1988).
3. Albert M., et al. *Nature*, **370**, 199 (1994).
4. Ebert M., et al. *Lancet*, **347**, 1297 (1996).
5. Laloe F., Ledyuk M., Nashe P.Zh., Novikov L.N., Tasteven J. *Usp. Fiz. Nauk.*, **147**, 433 (1985).
6. Papchenko A.A., Sobelman I.I., Yukov E.A. Preprint FIAN (24) (Moscow, 1989).
7. Kolachevsky N.N., Papchenko A.A., Prokofichev Yu.V., Skoi V.R., Sobelman I.I., Sorokin V.N. Preprint FIAN (39) (Moscow, 1999).
8. Kolachevsky N.N., Papchenko A.A., Prokhovichev Yu.V., Skoi V.R., Sobel'man I.I., Sorokin V.N. *Kvantovaya Electron.*, **30**, 81 (2000) [*Quantum Electron.*, **30**, 81 (2000)].
9. Cates G.D., Shaefer S.R., Happer W. *Phys. Rev. A*, **37**, 2877 (1988).
10. Skoy V.R., et al. *Nucl. Instr. Meth. Phys. Research A*, **402**, 232 (1998).
11. Sobelman I.I. *Atomic Spectra and Radiative Transitions* (New York: Springer Verlag, 1979).
12. Bethe H., Salpeter E. *Quantum Mechanics of Atoms with One and Two Electrons* (Moscow: Fizmatgiz, 1960).
13. Cowan R.D. *The Theory of Atomic Structure and Spectra* (Berkeley: University of California Press, 1981).
14. Cates G.D., et al. *Phys. Rev. A*, **45**, 4631 (1992).